Warren (2008), A depleted, not ideally chondritic bulk Earth: the explosive-volcanic basalt loss hypothesis — Electronic Annex

Introduction

The numbering, titles, and title formats for the various sections of this annex are chosen to denote the sections in the main paper to which these materials primarily relate.

3. Detailed Discussion of Analog Pyroclast Sizes

The dominant sizes of liquid blobs produced during eruption of explosively gas-charged magmas are difficult to predict on theoretical grounds. Klug and Cashman (1996) argued that the eruption rate has a controlling influence on blob size: a slow eruption rate allows time for gas permeability to develop in the ascending magma, which leads to early escape of most of the gas and a relatively low yield of fine melt blobs; conversely, a fast eruption rate favors efficient fragmentation of the eruptive matter into fine blobs. Eichelberger (1995) and Gonnermann and Manga (2003) argued that melt rheology is key: high viscosity favors development of intermittent permeable fracture networks (by "non-explosive fragmentation") near conduit walls, which leads to early escape of the gas and limits potential for efficient fragmentation into fine blobs. Wilson and Keil (1996) claimed that calculations (unspecified in nature, but presumably based on factors such as assumed eruption rate (cf. Wilson and Head, 2003) and rheology) indicate that the melt blobs produced by eruption of asteroidal basalt must be between ~30 and ~4000 μm in *d*.

Lacking a strong theoretical basis for predicting asteroidal pyroclastic melt drop sizes, we can turn to analogs from the Moon, Io and Earth. For the Moon, including pyroclastic glasses scattered in the lunar regolith and thereby sampled at all six Apollo landing sites (Shearer and Papike, 1993) as well as lunaite regolith breccias (Arai and Warren, 1999), many tens of discrete eruptive cycles appear to be represented. Among all of these different eruptions, the sizes of the pyroclasts were remarkably consistent, with *d* usually within a factor of five of 100 μm. For example, Arndt et al. (1987) found that for the Apollo-15 "green" glasses the median *d* is ~180 μm, and 99% have *d* <400 μm. These Apollo-15 green glasses probably represent multiple eruptive cycles, because several distinct compositional groupings can be distinguished (Delano, 1986; Shearer and Papike, 1993). However, Steele (1992) found that mean spheroid size is identical within a factor of 1.8 (in mass) among five distinct Apollo-15 green subtypes. Arndt et al. (1987) found that for the Apollo-17 "orange-black" glassy pyroclastic spheroids (which are in many cases largely crystalline, and again, represent several distinct compositional groupings (Shearer and Papike, 1993)) the median *d* is ~150 μm and 99%

have d <250 μm. I have also noted a very similar size distribution for the black spheroids that compose tuff-breccia 72504,10, a rocklet collected over 4 km away from the Shorty Crater sampling station where Apollo-17 pyroclasts were primarily sampled (Jerde et al., 1987).

The size-frequency distributions for other pyroclastic mare glasses are so similar to those for the Apollo-15 and Apollo-17 pyroclastic glasses (the author's personal observations over many years of innumerable regolith petrographic samples as well as sample-description presentations by colleagues such as J. W. Delano) that descriptions of pyroclastic glasses in new contexts (e.g., regolith-breccia lunaites) seldom bother to note the spherule sizes. For the several distinct varieties from Apollo 14, Shearer et al. (1989) noted that the spheroids are generally 10-100 μm in "size" (d); i.e., if anything, smaller than their Apollo-17 counterparts. Based on limited statistics, Arai and Warren (1999) described an Apollo-17-like size distribution for pyroclastic spheroids in two launch-paired lunaite regolith breccias. The pyroclastic spheroids in the Dhofar 287 regolith breccia (the detailed petrology and compositions of these lunaites confirm the actuarial expectation that the launch sites were far from any Apollo site) are likewise described as 100 to 350 μm in "size" (d) (Demidova et al., 2003).

Wilson and Head (2003) suggested that the lunar pyroclastic eruptions were gas-rich, and thus pyroclastic, as a consequence of a distinctive style of magmatic ascent, during which a gas-rich foam would evolve at the top of dike-like rising magma parcels; and (implicitly) that the lava-parent magmas failed to develop topping foams to the same extent only because their ascents began at shallower depths. Wilson and Head (2003) claimed that this model accounts for the well-known lack of correspondence between pyroclastic glass types and lava types among lunar mare materials (Longhi, 1987). However, the lack of correspondence in question is not merely a lack of agreement between individual pyroclast types and lava types. The compositions of the pyroclastic glasses as an overall population are more MgO-rich (and Al_2O_3-depleted) by a factor of roughly 2 compared to the compositions of the sampled lavas as an overall population (Arai and Warren, 1999; lunar petrologists frequently use the terms "picritic glass" and pyroclastic glass as synonyms). It therefore appears unlikely that the gas-rich nature of the pyroclastic eruptions arose purely from a difference in the style of magmatic ascent toward the surface. Arai and Warren (1999) suggested that the source materials of the pyroclastic picrites were lunar mantle locales of more generally primitive character than the lava source materials; and that high volatile (C, graphite) content was associated with high MgO in these primitive materials. An association between graphite and overall primitiveness makes sense, because graphite's low density (2,200 kg m^{-3}) must have resulted in efficient depletion from all but the shallowest portion of the magma ocean. For present purposes, the only important

difference between these models is that the magma's initial volatile content is even more crucial for determining whether an eruption is pyroclastic or not in the Arai and Warren (1999) model than in the Wilson and Head (2003) model. Wilson and Keil (1997) acknowledged that the chief reason pyroclastics are absent among HED meteorites (which are similar in many respects to lunar mare materials) is probably the low content of volatiles (including C) characteristic of the HED-parent asteroid.

It may be significant that during lunar pyroclastic eruptions bubble nucleation and growth were controlled by diffusion of oxygen from the melt onto surfaces of oxidizing graphite grains, rather than (as in classical pyroclastic eruption modeling) by homogeneous nucleation and growth from volatile species such as H_2O or CO_2, exsolved from supersaturated melt. This ready availability of nucleation surfaces may have contributed to the tendency for lunar pyroclastic size distributions to be well-sorted, both within individual eruptive ensembles (Arndt et al., 1987), and as an overall population of materials.

The silicate pyroclasts of Io are discussed in the main text. Earth, with its atmosphere and its tendency for volatile-rich magmas to be viscous-rhyolitic, makes a poor analog. However, it is worth noting that where total grain size distributions have been estimated for very large terrestrial pyroclastic plumes, in most instances at least 70 wt% of the pyroclastic matter is finer than 2 mm in *d* (Walker, 1981; Carey and Sigurdsson, 1982; Koyaguchi and Ohno, 2001).

6. Model Results

6.3. Application of stoichiometry to constrain depletion of Al_2O_3 and CaO

The depletions CaO and Al_2O_3 can be estimated by simple application of stoichiometry. Four main parameters need to be estimated: the initial composition (presumably broadly chondritic), the proportion of basalt lost (the *f* or *X* at which pyroclastic blow-off ceases, in our reference model), the proportion of plagioclase in the melting that formed the blown-off basalt (0.6, in our reference model), and the mean composition of that plag (pure anorthite has 36.6 wt% Al_2O_3 and 20.2 wt% CaO; pure albite has 19.4 wt% Al_2O_3 and zero CaO). Of course, one additional key parameter for modeling the final-Earth composition is the unfractionated proportion *Y* (as discussed above, the *Y* component and the initial matter before basalt dissipation are assumed to be compositionally identical).

Various data from equilibrated chondrites (Fredriksson et al., 1975; Dube et al., 1977; Hutchison et al., 1981) as well as ureilites (Kita et al., 2004; Warren et al., 2006) all suggest that plag melted in our scenario would be highly albitic, e.g., An_{10}-An_{20}. The CIPW-normative plag of the final Earth,

according to typical estimates of the "primitive mantle" composition (Warren, 2005) is more calcic, An_{75}. However, the CIPW calculation (which determines anorthite based on the Al_2O_3 left after allocation to orthoclase + albite) ignores the role of pyroxene as an important reservoir for Al_2O_3 (and Na_2O) in real ultramafic rocks. Also, the well-known tendency for Na to be relatively (compared to Ca) incompatible implies the residuum will be Na/Ca-depleted compared to the original material. On balance, a melting-plag composition of An_{20}-An_{30} seems most plausible. However, models have been calculated for the range An_{10}-An_{40}.

6.5. Wider Departures from the Reference Model

The full range of parameter-space conceivably relevant to the hypothesis of explosive-volcanic basalt loss is too complex to cover in detail within the scope of a single paper. However, Tables EA-1 and EA-2 (expanded versions of Tables 2 and 3 of the main text) show $(Nd/Sm)_Y$ and other key results from a selection of models meant to cover the range of plausible variations in salient parameters.

Variation in Φ: The batch melting models of Figs. 3a, 3c and 4 assume a low residual porosity Φ. Increasing Φ dampens all net residuum fractionations, so that for any given f (in the ~ 0-0.2 range of interest) the final-Earth Nd/Sm is significantly higher. Increasing Φ from 0.005 in Fig. 3c to 0.03 in Fig. 3d has the effect of increasing $(Nd/Sm)_{0.60}$ from 0.933 to 0.961. However, this effect on Nd/Sm is to some degree offset by parallel dampening of other fractionations, the net effect of which allows a considerably lower Y to be assumed without implying implausibly large fractionations between Th (and U) and less incompatible elements, or large fractionations involving Al_2O_3 and CaO, etc. Taking Eu as an example, assuming 30 wt% initial olivine, as in Fig. 3c, the f for complete elimination of the residuum's Eu anomaly is identical (0.060, assuming $K_{Eu,plag} = 0.7$) for Φ = 0.03 as it is for Φ = 0.005, but the amount of basalt lost, at this f, is 1.8 times greater with Φ = 0.005 as with Φ = 0.03.

The effect of changing from Φ = 0.005 to Φ = 0.03 in dynamic melting is shown by contrasting Figs. 5a vs. 5b, or 5c vs. 5d. The effect of higher Φ is to make the dip in the final-Earth Nd/Sm curve shallower but also broader. The dampened Nd/Sm fractionation is in itself a drawback, but one that is more than offset by the broadening of the Nd/Sm dip, plus dampening of other fractionations, including the Eu anomaly, such that even a Y of 0.5 does not imply drastic fractionation of Al_2O_3, Al/Ca, Th/Ca, etc. Although Figs. 5a and 5c, with Φ = 0.005, are included for completeness, such a low Φ in dynamic melting may be unrealistic in the low-gravity setting of a planetesimal (the batch melting model, with the removal of melt happening through single episode of abrupt, turbulent movement of melt and its surrounding solids, might more plausibly engender a low final porosity).

Even assuming that a low dynamic Φ occurred, it would probably entail seepage of melt through extremely narrow channels, and as such might not be conducive to the significant entrainment of solid graphite that is a major premise of the basalt blow-off model. Other volatiles could potentially contribute to basalt blow-off, but graphite is clearly the most potentially effective fuel for explosive volcanism in this context.

Initial modal pyroxene/olivine ratio: The influence of the initial modal pyroxene/olivine ratio on batch-style melting is illustrated by contrasting Fig. 3a vs. 3c; or 3b vs. 3d. High pyroxene/olivine is an advantage, both in terms of Nd/Sm, per se, and in terms of attainment of a negligible Eu anomaly (assuming this is truly an advantage) at relatively low *f*. Under the dynamic melting scenario, unless Φ is at least moderately high, the 50 wt% olivine variant of the reference model is problematic, with a considerable (+) Eu anomaly persisting until high *f*, by which point Nd/Sm is little-fractionated, while Al_2O_3 and Al/Ca ratio are greatly fractionated. However, as dynamic Φ increases past ~0.02, these drawbacks become less severe. For example, in comparing Figs. 5a (Φ = 0.005) and 5b (Φ = 0.03), the optimal *f,* from a Eu anomaly minimization standpoint, is nearly the same, but the fraction of basalt lost *X* decreases from (assuming *Y* = 0.60) 0.116 to 0.086. Also, the drawbacks associated with low *Y* (strong fractionations in ratios such as Al/Ca and Th/Lu) are mitigated by the high Φ.

Initial modal pigeonite: According to Longhi and Pan (1988), pigeonite is unlikely to be abundant, relative to a combination of opx + high-Ca pyroxene, at the high *mg* of typical Earth protoplanets. Among high-*mg* igneous-restitic meteorites, the pyroxenes in the aubrites (enstatite + diopside) as well as the lodranites (opx + augite) conform to the Longhi and Pan (1988) model. However, even some of the most magnesian (in one case Fo_{95}) ureilites contain pigeonite (Mittlefehldt et al., 1998).

Although substituting a moderate proportion of pigeonite for opx + augite would leave Figs. 3 and 5 looking qualitatively little-changed, the effects (assuming available *K* values are valid) are potentially significant. In both the batch melting and the dynamic scenarios, pigeonite dampens Nd/Sm fractionation in the restite for any given *f*, and also causes the restite to retain a positive Eu anomaly to higher *f* compared to otherwise analogous models with zero pigeonite. For example, in a batch-type model analogous to Fig. 3a but assuming 20 wt% initial pigeonite, $(Nd/Sm)_{60}$ increases by 0.018 (to 0.967). In a Fig. 3c analog, assuming 20 wt% initial pigeonite increases $(Nd/Sm)_{60}$ by 0.009 (to 0.942).

In a dynamic melting model otherwise analogous to Fig. 5b assuming 20 wt% initial pigeonite increases $(Nd/Sm)_{55}$ by 0.027 (to 0.977). In a Fig. 5c analog, increasing the initial pigeonite to 20

wt% increases $(Nd/Sm)_{55}$ by 0.059 (to 0.965). In a Fig. 5d analog, increasing the initial pigeonite to 20 wt% increases $(Nd/Sm)_{55}$ by 0.007 (to 0.941). As this comparison indicates, pigeonite's influence is more decisive among low-Φ dynamic-type models than among high-Φ ones.

Initial modal plagioclase: There is relatively little scope for variation in initial modal plagioclase (assuming broadly chondritic starting material). Still, the effects are conceivably important. In batch-melting-based models analogous to Fig. 3a, $(Nd/Sm)_{60}$ decreases to 0.938 when initial plag is decreased to 8 wt%, or increases to 0.959 if initial plag is increased to 12 wt%. In Fig. 3c analog models, $(Nd/Sm)_{60}$ is little changed (0.932-0.938) with initial plag varied over the range 8-12 wt%. In dynamic-melting-based models analogous to Fig. 5b, an initial plag range of 8-12 wt% corresponds to $(Nd/Sm)_{55}$ from 0.944 to 0.971. In a Fig. 5c analog, an initial plag range of 8-12 wt% corresponds to $(Nd/Sm)_{55}$ from 0.883 to 0.958. In a Fig. 5d analog, 8 wt% initial plag increases $(Nd/Sm)_{55}$ to 0.972; 12 wt% initial plag leaves $(Nd/Sm)_{55}$ virtually unchanged at 0.933.

Modal melting pyroxene/plag ratio: As discussed above, the Na-rich, high-*mg* initial composition assumed for the initial Earth-protoplanet materials implies a high plag/(plag+pyroxene) ratio of conservatively 0.6 for the matter that undergoes melting. Fortunately, except for the unlikely case of low-Φ dynamic melting, varying the modal melting pyroxene/plag ratio does not dramatically affect key results such as $(Nd/Sm)_Y$. In batch-melting-based models analogous to Fig. 3a, a range of 0.3-0.5 for the melting pyroxene/(plag+pyroxene) ratio corresponds to a $(Nd/Sm)_{60}$ range of 0.944 to 0.955. In models analogous to Fig. 3c, varying the melting pyroxene/(plag+pyroxene) ratio from 0.5 to 0.3 leaves $(Nd/Sm)_{60}$ virtually unchanged (0.932 to 0.933). In dynamic-melting-based models analogous to Fig. 5b, a range of 0.3-0.5 for the melting pyroxene/(plag+pyroxene) ratio corresponds to a $(Nd/Sm)_{55}$ range of 0.944 to 0.963. In a Fig. 5c analog, a range of 0.3-0.5 for the melting pyroxene/(plag+pyroxene) ratio corresponds to $(Nd/Sm)_{55}$ from 0.893 to 0.926. In a Fig. 5d analog, a range of 0.3-0.5 for the melting pyroxene/(plag+pyroxene) ratio corresponds to $(Nd/Sm)_{55}$ from 0.931 to 0.943.

Magnitude of the unfractionated (Y) component: The influence of *Y* on the final-Earth composition is easily understood and has already been covered, passim, above. Assuming a too high *Y* dampens fractionations, including Nd/Sm, toward insignificance. Assuming a too low *Y* has the drawback of predicting extreme fractionations in ratios such as Al/Ca and Th/Lu. Depending upon the other model parameters, in particular Φ (which acts a little like *Y*, in terms of dampening fractionations), in practice the most successful models, in terms of matching the apparent bulk-Earth Nd/Sm of 0.932 times chondritic (Boyet and Carlson, 2006) without implausibly extreme

concomitant fractionations, are limited to a relatively narrow range of assumed Y (~0.50-0.65). However, it must be recalled that the assumption of 2-component mixing, between an unfractionated Y component and a single variety of thoroughly fractionated planetesimals, is merely an expedient to keep the modeling tractable and the results comprehensible. The real-world scenario would involve diverse extents of fractionation among individual planetesimals. The various problems associated with low Y are genuine concerns for the model, because they represent drawbacks to over-fractionation of the protoearths. But to assume a "too high" Y is just another way of saying the obvious fact that the proposed mechanism (protoplanet basalt dissipation by explosive volcanism) might not be highly efficient. The single drawback of high-Y models, limited bulk-Earth Nd/Sm (etc.) fractionation, still seems preferable, in light of recent ε_{Nd} data, versus zero bulk-Earth Nd/Sm fractionation.

Variation in $K_{Eu,plag}$: The effects of a higher $K_{Eu,plag}$ are generally disadvantageous. In batch-melting-based models analogous to Fig. 3a, an increase in $K_{Eu,plag}$ to 1.1 results in $(Nd/Sm)_{60}$ increasing to 0.973. In models analogous to Fig. 3c, a $K_{Eu,plag}$ of 1.1 results in $(Nd/Sm)_{60}$ raised to 0.963. In dynamic-melting-based models analogous to Fig. 5b, a $K_{Eu,plag}$ of 1.1 results in $(Nd/Sm)_{55}$ increased all the way to 0.991. In a Fig. 5c analog, the effect is to raise $(Nd/Sm)_{55}$ to 0.954. However, in a Fig. 5d analog, the effect on $(Nd/Sm)_{55}$ is a slight decrease from 0.934 to 0.931. Assuming Eu anomaly minimization is a key goal, a higher $K_{Eu,plag}$ can be a slight advantage in the case of melting (batch or dynamic) with a very high Φ, because the minimum in the trend of final-Earth Nd/Sm as a function of f (or of X ($\approx f - \Phi$)) in such a case does not come until beyond the f of Eu/Eu* = 1 with $K_{Eu,plag} = 0.7$.

References

Arai T. and Warren P. H. (1999) Lunar meteorite QUE94281: Glass compositions and other evidence for launch pairing with Yamato-793274. *Meteor. Planet. Sci*. **34**, 209-234.

Arndt J. and von Englehardt W. (1987) Formation of Apollo 17 orange and black glass beads. *Proc. Lunar Planet. Sci. Conf.* **17**, E372-E376.

Boyet M. and Carlson R. W. (2006) A new geochemical model for the Earth's mantle inferred from ^{146}Sm-^{142}Nd systematics. *Earth Planet. Sci. Lett*. **250**, 254-268.

Carey S. N. and Sigurdsson H. (1982) Influence of particle aggregation on deposition of distal tephra from the May 18, 1980, eruption of Mount St. Helens volcano. *J. Geophys. Res*. **87**, 7061-7072.

Delano J. W. (1986) Pristine lunar glasses: Criteria, data, and implications. *Proc. Lunar Planet. Sci. Conf.* **16**, D201-D213.

Demidova S. I., Nazarov M. A., Anand M. and Taylor L. A. (2003) Lunar regolith breccia Dhofar 287B: A record of lunar volcanism. *Meteor. Planet. Sci.* **38**, 501-514.

Dube A., Fredriksson B. J., Jarosewich E., Nelen J. A., Noonan A. F., O'Keefe J. and Fredriksson K. (1977)

Eight L-group chondrites: A comparative study. *Smithson. Contrib. Earth Sci.* **19**, 71-82.

Eichelberger J. C. (1995) Silicic volcanism: ascent of viscous magmas from crustal reservoirs. *Ann. Rev. Earth Planet. Sci.* **23**, 41-63.

Fredriksson K., Dube A., Jarosewich E., Nelen J. and Noonan A. (1975) The Pulsora anomaly: A case against metamorphic equilibration in chondrites. Smithson. Contrib. Earth Sci. 14, 41-53.

Gonnermann H. M. and Manga M. (2003) Explosive volcanism may not be an inevitable consequence of magma fragmentation. *Nature* **426**, 432-435.

Hutchison R., Bevan A. W. R., Easton A. J. and Agrell S. O. (374) Mineral chemistry and genetic relations among H-group chondrites. *Proceedings of the Royal Society of London, Series A, Mathematical and Physical Sciences* **374**, 159-178.

Jerde E. A., Warren P. H., Morris R. V., Heiken G. H. and Vaniman D. T. (1987) A potpourri of regolith breccias: "New" samples from the Apollo 14: 16 and 17 landing sites. *Proc. Lunar Planet. Sci. Conf.* **17**, E526-E536.

Kita N. T., Ikeda Y., Togashi S., Liu Y., Morishita Y. and Weisberg M. K. 2004. Origin of ureilites inferred from a SIMS oxygen isotopic and trace element study of clasts in the Dar al Gani 319 polymict ureilite. *Geochimica et Cosmochimica Acta* 68:4213-4235.

Klug C. and Cashman K. V. (1996) Permeability development in vesiculating magmas: implications for fragmentation. *Bullet. Volcanol.* **58**, 87-100.

Koyaguchi T. and Ohno M. (2001) Reconstruction of eruption column dynamics on the basis of grain size of tephra fall deposits. 1. Methods. *J. Geophys. Res*. **106**, 6499-6512.

Longhi J. (1987) On the connection between mare basalts and picritic volcanic glasses. *Proc. Lunar Planet. Sci. Conf.* **17**, E349-E360.

Longhi J. and Pan V. (1988) A reconnaissance study of phase boundaries in low-alkali basaltic liquids. *Jour. Petrol.* **29**, 115-147.

Mittlefehldt D. W., McCoy T. J., Goodrich C. A. and Kracher A. (1998) Non-chondritic meteorites from asteroidal bodies. *Reviews Mineral. Geochem*. **36**, 4.1-4.195.

Sato M. (1979) The driving mechanism of lunar pyroclastic eruptions inferred from the oxygen fugacity behavior of Apollo 17 orange glass. *Proc. Lunar Planet. Sci. Conf.* **10**, 311-325.

Shearer C. K. and Papike J. J. (1993) Basaltic magmatism on the Moon: A perspective from volcanic picritic glass beads. *Geochim. Cosmochim. Acta* **57**, 4785-4812.

Shearer C. K., Papike J. J., Simon S. B., Shimizu N., Yurimoto H. and Sueno S. (1989) An ion microprobe study of trace elements in Apollo 14 "volcanic" glass beads and comparisons to mare basalts. In *Workshop on Moon in Transition: Apollo 14, KREEP, and Evolved Lunar Rocks* (eds. G. J. Taylor and P. H. Warren), pp. 113-117. Lunar and Planetary Institute Technical Report 89-03.

Steele A. M. (1992) Apollo 15 green glass: Relationships between texture and composition. *Proc. Lunar Planet. Sci. Conf.* **22**, 329-341.

Walker G. P. L. (1981) Generation and dispersal of fine ash and dust by volcanic eruptions. *Jour. Volcan. Geotherm. Res.* **11**, 81-92.

Warren P. H. (2005) "New" lunar meteorites: Implications for composition of the global lunar surface, of the lunar crust, and of the bulk Moon. *Meteor. Planet. Sci.* **40**, 477-506.

Warren P. H., Ulff-Møller F., Huber H. and Kallemeyn G. W. (2006) Siderophile geochemistry of ureilites: a record of early stages of planetesimal core formation. *Geochim. Cosmochim. Acta* **70**, 2104-2126.

Weitz C. M., Rutherford M. J., Head J. W. III and McKay D. S. (1999) Ascent and eruption of a lunar high-titanium magma as inferred from the petrology of the 74001/2 drill core. *Meteor. Planet. Sci*. **34**, 527-

540.

Wilson L. and Head J. W., III (2003) Deep generation of magmatic gas on the Moon and implications for pyroclastic eruptions. *Geophys. Res. Lett.* **30**, 7.1-7.4.

Wilson L. and Keil K. (1996) Volcanic eruptions and intrusions on the asteroid 4 Vesta. *J. Geophys. Res. Planets* **101**, 18927-18940.

Wilson L. and Keil K. (1997) The fate of pyroclasts produced in explosive eruptions on the asteroid 4 Vesta. *Meteor. Planet. Sci.* **32**, 813-823.

Table EA-1. Results from a selection of batch-melting based models.

entering	initial fraction			melt	residual	melt	mixing	final-Earth composition											
melt plag	olvn	pigeon	plag	*f*	Φ	*X*	*Y*	Th	Hf	La	Nd	Sm	Eu	Gd	Lu	Nd/Sm	Eu/Eu*	Eu^a/Eu*	Al/Ca
0.6	0.5	0	0.10	0.094	0.005	0.089	0.50	0.529	0.650	0.550	0.593	0.638	0.668	0.686	0.827	0.929	1.010	1.079	0.814
0.6	0.5	0	0.10	0.091	0.005	0.086	0.60	0.624	0.723	0.641	0.676	0.713	0.739	0.751	0.865	0.949	1.010	1.061	0.858
0.6	0.5	0	0.10	0.088	0.005	0.083	0.70	0.719	0.795	0.732	0.759	0.787	0.810	0.816	0.901	0.964	1.010	1.046	0.900
0.6	0.5	0	0.10	0.090	0.03	0.061	0.50	0.669	0.757	0.685	0.716	0.749	0.773	0.782	0.882	0.957	1.010	1.053	0.877
0.6	0.5	0	0.10	0.086	0.03	0.058	0.60	0.741	0.812	0.754	0.779	0.805	0.827	0.832	0.910	0.968	1.010	1.043	0.909
0.6	0.5	0	0.10	0.080	0.03	0.052	0.70	0.814	0.867	0.824	0.843	0.862	0.881	0.882	0.938	0.977	1.010	1.033	0.941
0.6	0.3	0	0.10	0.051	0.005	0.046	0.50	0.555	0.756	0.605	0.691	0.759	0.795	0.816	0.924	0.910	1.010	1.070	0.911
0.6	0.3	0	0.10	0.048	0.005	0.043	0.60	0.647	0.813	0.690	0.761	0.815	0.845	0.860	0.943	0.933	1.010	1.054	0.935
0.6	0.3	0	0.10	0.041	0.005	0.036	0.70	0.741	0.872	0.777	0.833	0.874	0.898	0.906	0.963	0.953	1.010	1.039	0.960
0.6	0.3	0	0.10	0.073	0.03	0.044	0.50	0.709	0.816	0.731	0.777	0.818	0.828	0.854	0.934	0.951	0.990	1.028	0.916
0.6	0.3	0	0.10	0.076	0.03	0.047	0.60	0.760	0.846	0.777	0.815	0.847	0.854	0.878	0.944	0.961	0.990	1.020	0.927
0.6	0.3	0	0.10	0.081	0.03	0.053	0.70	0.813	0.877	0.825	0.853	0.878	0.881	0.902	0.954	0.972	0.990	1.012	0.939
0.6	0.5	0.20	0.10	0.121	0.005	0.116	0.50	0.523	0.609	0.532	0.559	0.587	0.609	0.620	0.762	0.953	1.010	1.063	0.752
0.6	0.5	0.20	0.10	0.119	0.005	0.114	0.60	0.618	0.689	0.626	0.648	0.671	0.691	0.698	0.811	0.967	1.010	1.049	0.809
0.6	0.5	0.20	0.10	0.115	0.005	0.111	0.70	0.714	0.768	0.721	0.737	0.754	0.772	0.775	0.861	0.977	1.010	1.038	0.864
0.6	0.5	0.20	0.10	0.118	0.03	0.091	0.50	0.628	0.697	0.636	0.658	0.679	0.699	0.706	0.816	0.968	1.010	1.048	0.809
0.6	0.5	0.20	0.10	0.116	0.03	0.088	0.60	0.705	0.760	0.712	0.729	0.746	0.765	0.768	0.856	0.976	1.010	1.039	0.855
0.6	0.5	0.20	0.10	0.111	0.03	0.084	0.70	0.782	0.824	0.787	0.800	0.814	0.830	0.830	0.895	0.984	1.010	1.031	0.899
0.6	0.3	0.20	0.10	0.081	0.005	0.076	0.50	0.535	0.680	0.560	0.619	0.672	0.706	0.726	0.867	0.921	1.010	1.079	0.843
0.6	0.3	0.20	0.10	0.079	0.005	0.074	0.60	0.629	0.747	0.650	0.698	0.741	0.770	0.784	0.896	0.942	1.010	1.061	0.880
0.6	0.3	0.20	0.10	0.074	0.005	0.070	0.70	0.723	0.814	0.740	0.777	0.810	0.834	0.843	0.925	0.960	1.010	1.046	0.917
0.6	0.3	0.20	0.10	0.097	0.03	0.069	0.50	0.658	0.753	0.672	0.711	0.747	0.758	0.785	0.890	0.952	0.990	1.031	0.860
0.6	0.3	0.20	0.10	0.099	0.03	0.072	0.60	0.723	0.798	0.734	0.765	0.793	0.800	0.824	0.909	0.964	0.990	1.021	0.885
0.6	0.3	0.20	0.10	0.104	0.03	0.076	0.70	0.788	0.844	0.796	0.819	0.840	0.843	0.863	0.928	0.975	0.990	1.011	0.909
0.6	0.5	0	0.08	0.054	0.005	0.049	0.50	0.551	0.723	0.585	0.652	0.711	0.745	0.765	0.892	0.916	1.010	1.076	0.905
0.6	0.5	0	0.08	0.051	0.005	0.046	0.60	0.643	0.783	0.671	0.726	0.774	0.803	0.817	0.917	0.938	1.010	1.059	0.929
0.6	0.5	0	0.08	0.047	0.005	0.043	0.70	0.735	0.843	0.758	0.800	0.837	0.861	0.869	0.942	0.956	1.010	1.044	0.952
0.6	0.5	0	0.08	0.070	0.03	0.041	0.50	0.718	0.809	0.733	0.768	0.802	0.810	0.834	0.918	0.958	0.990	1.024	0.923
0.6	0.5	0	0.08	0.072	0.03	0.044	0.60	0.768	0.841	0.780	0.808	0.835	0.840	0.862	0.931	0.968	0.990	1.017	0.934
0.6	0.5	0	0.08	0.076	0.03	0.048	0.70	0.819	0.874	0.828	0.849	0.869	0.871	0.889	0.944	0.976	0.990	1.009	0.945
0.6	0.3	0	0.08	0.032	0.005	0.027	0.50	0.588	0.823	0.654	0.759	0.827	0.842	0.875	0.954	0.918	0.990	1.037	0.954
0.6	0.3	0	0.08	0.034	0.005	0.029	0.60	0.666	0.851	0.715	0.799	0.853	0.865	0.894	0.960	0.936	0.990	1.028	0.959
0.6	0.3	0	0.08	0.038	0.005	0.033	0.70	0.744	0.880	0.779	0.840	0.882	0.888	0.913	0.967	0.953	0.990	1.019	0.964
0.6	0.3	0	0.08	0.046	0.03	0.016	0.50	0.831	0.913	0.850	0.887	0.914	0.915	0.936	0.974	0.970	0.990	1.009	0.979
0.6	0.3	0	0.08	0.049	0.03	0.019	0.60	0.850	0.920	0.866	0.897	0.921	0.922	0.941	0.976	0.974	0.990	1.007	0.977
0.6	0.3	0	0.08	0.053	0.03	0.024	0.70	0.872	0.929	0.884	0.910	0.930	0.929	0.947	0.978	0.978	0.990	1.004	0.977
0.6	0.5	0	0.12	0.133	0.005	0.129	0.50	0.521	0.612	0.535	0.566	0.600	0.626	0.639	0.777	0.942	1.010	1.074	0.724
0.6	0.5	0	0.12	0.131	0.005	0.126	0.60	0.617	0.691	0.628	0.654	0.682	0.704	0.713	0.824	0.959	1.010	1.057	0.788
0.6	0.5	0	0.12	0.127	0.005	0.122	0.70	0.713	0.770	0.722	0.742	0.763	0.782	0.787	0.870	0.972	1.010	1.043	0.850
0.6	0.5	0	0.12	0.131	0.03	0.104	0.50	0.616	0.691	0.628	0.653	0.681	0.704	0.713	0.823	0.959	1.010	1.057	0.781
0.6	0.5	0	0.12	0.127	0.03	0.100	0.60	0.695	0.756	0.705	0.726	0.748	0.768	0.773	0.862	0.970	1.010	1.045	0.834
0.6	0.5	0	0.12	0.122	0.03	0.095	0.70	0.774	0.820	0.782	0.798	0.815	0.832	0.834	0.900	0.979	1.010	1.035	0.884
0.6	0.3	0	0.12	0.091	0.005	0.087	0.50	0.531	0.678	0.561	0.623	0.680	0.715	0.736	0.871	0.915	1.010	1.083	0.819
0.6	0.3	0	0.12	0.088	0.005	0.084	0.60	0.626	0.746	0.651	0.701	0.747	0.777	0.792	0.900	0.938	1.010	1.064	0.863
0.6	0.3	0	0.12	0.083	0.005	0.079	0.70	0.720	0.813	0.740	0.779	0.815	0.840	0.849	0.928	0.956	1.010	1.048	0.905
0.6	0.3	0	0.12	0.086	0.03	0.058	0.50	0.677	0.782	0.699	0.743	0.784	0.811	0.823	0.915	0.948	1.010	1.055	0.885
0.6	0.3	0	0.12	0.081	0.03	0.053	0.60	0.750	0.835	0.769	0.804	0.836	0.860	0.867	0.937	0.962	1.010	1.043	0.918
0.6	0.3	0	0.12	0.070	0.03	0.042	0.70	0.830	0.893	0.844	0.870	0.894	0.913	0.915	0.961	0.974	1.010	1.031	0.953
0.5	0.5	0	0.10	0.116	0.005	0.112	0.50	0.523	0.626	0.540	0.575	0.614	0.641	0.656	0.797	0.937	1.010	1.077	0.762
0.5	0.5	0	0.10	0.113	0.005	0.109	0.60	0.619	0.703	0.633	0.662	0.693	0.717	0.727	0.840	0.955	1.010	1.059	0.819
0.5	0.5	0	0.10	0.109	0.005	0.104	0.70	0.715	0.780	0.726	0.748	0.773	0.793	0.799	0.883	0.969	1.010	1.044	0.873
0.5	0.5	0	0.10	0.113	0.03	0.085	0.50	0.635	0.715	0.648	0.676	0.706	0.729	0.739	0.847	0.957	1.010	1.057	0.822
0.5	0.5	0	0.10	0.109	0.03	0.081	0.60	0.712	0.777	0.722	0.745	0.770	0.790	0.796	0.882	0.968	1.010	1.045	0.868
0.5	0.5	0	0.10	0.102	0.03	0.074	0.70	0.789	0.840	0.798	0.816	0.834	0.853	0.854	0.917	0.978	1.010	1.035	0.912
0.7	0.5	0	0.10	0.078	0.005	0.073	0.50	0.535	0.673	0.560	0.610	0.661	0.692	0.711	0.851	0.924	1.010	1.080	0.850
0.7	0.5	0	0.10	0.076	0.005	0.071	0.60	0.629	0.740	0.649	0.690	0.731	0.758	0.771	0.883	0.944	1.010	1.062	0.885
0.7	0.5	0	0.10	0.073	0.005	0.068	0.70	0.723	0.808	0.738	0.770	0.801	0.824	0.832	0.915	0.961	1.010	1.046	0.919
0.7	0.5	0	0.10	0.074	0.03	0.045	0.50	0.706	0.796	0.723	0.756	0.789	0.813	0.821	0.909	0.958	1.010	1.049	0.914
0.7	0.5	0	0.10	0.070	0.03	0.041	0.60	0.773	0.845	0.787	0.813	0.839	0.860	0.864	0.932	0.969	1.010	1.039	0.938
0.7	0.5	0	0.10	0.063	0.03	0.034	0.70	0.843	0.896	0.854	0.874	0.892	0.910	0.910	0.956	0.979	1.010	1.029	0.963
0.5	0.3	0	0.10	0.064	0.005	0.059	0.50	0.544	0.725	0.585	0.662	0.727	0.763	0.785	0.905	0.910	1.010	1.077	0.881
0.5	0.3	0	0.10	0.060	0.005	0.055	0.60	0.638	0.787	0.673	0.736	0.789	0.820	0.835	0.929	0.933	1.010	1.059	0.913
0.5	0.3	0	0.10	0.053	0.005	0.048	0.70	0.732	0.850	0.761	0.812	0.852	0.877	0.886	0.952	0.953	1.010	1.043	0.945
0.5	0.3	0	0.10	0.088	0.03	0.060	0.50	0.672	0.778	0.693	0.738	0.780	0.791	0.820	0.914	0.947	0.990	1.033	0.879
0.5	0.3	0	0.10	0.092	0.03	0.064	0.60	0.732	0.816	0.748	0.784	0.817	0.825	0.850	0.927	0.959	0.990	1.023	0.897
0.5	0.3	0	0.10	0.099	0.03	0.071	0.70	0.793	0.855	0.804	0.831	0.856	0.859	0.880	0.941	0.971	0.990	1.014	0.916

Table EA-2. Results from a selection of dynamic-melting based models.

entering	initial fraction			melt	residual	melt	mixing	final-Earth composition											
melt plag	olvn	pigeon	plag	*f*	Φ	*X*	*Y*	Th	Hf	La	Nd	Sm	Eu	Gd	Lu	Nd/Sm	Eu/Eu*	Eu^a/Eu*	Al/Ca
0.6	0.5	0	0.10	0.123	0.005	0.119	0.50	0.500	0.506	0.500	0.501	0.511	0.530	0.540	0.705	0.980	1.010	1.072	0.747
0.6	0.5	0	0.10	0.120	0.005	0.116	0.60	0.600	0.605	0.600	0.601	0.610	0.628	0.634	0.768	0.985	1.010	1.056	0.807
0.6	0.5	0	0.10	0.116	0.005	0.111	0.70	0.700	0.705	0.700	0.701	0.709	0.725	0.728	0.830	0.989	1.010	1.044	0.863
0.6	0.5	0	0.10	0.117	0.03	0.090	0.50	0.505	0.585	0.536	0.564	0.600	0.627	0.642	0.778	0.941	1.010	1.066	0.812
0.6	0.5	0	0.10	0.114	0.03	0.086	0.60	0.605	0.674	0.633	0.656	0.685	0.709	0.719	0.828	0.957	1.010	1.051	0.859
0.6	0.5	0	0.10	0.108	0.03	0.080	0.70	0.706	0.763	0.729	0.749	0.772	0.792	0.798	0.878	0.970	1.010	1.039	0.904
0.6	0.3	0	0.10	0.080	0.005	0.075	0.50	0.500	0.574	0.501	0.530	0.596	0.638	0.671	0.838	0.890	1.010	1.112	0.845
0.6	0.3	0	0.10	0.077	0.005	0.072	0.60	0.600	0.665	0.601	0.627	0.682	0.719	0.743	0.875	0.920	1.010	1.083	0.884
0.6	0.3	0	0.10	0.072	0.005	0.067	0.70	0.700	0.756	0.701	0.725	0.769	0.800	0.816	0.912	0.943	1.010	1.060	0.921
0.6	0.3	0	0.10	0.082	0.03	0.053	0.50	0.549	0.712	0.617	0.678	0.732	0.749	0.782	0.883	0.925	0.990	1.041	0.895
0.6	0.3	0	0.10	0.086	0.03	0.057	0.60	0.632	0.759	0.683	0.731	0.776	0.788	0.816	0.901	0.943	0.990	1.029	0.910
0.6	0.3	0	0.10	0.092	0.03	0.064	0.70	0.717	0.807	0.752	0.787	0.820	0.828	0.852	0.919	0.960	0.990	1.018	0.925
0.6	0.5	0.20	0.10	0.141	0.005	0.137	0.50	0.500	0.501	0.500	0.500	0.501	0.510	0.508	0.633	0.998	1.010	1.032	0.706
0.6	0.5	0.20	0.10	0.138	0.005	0.133	0.60	0.600	0.601	0.600	0.600	0.601	0.610	0.607	0.710	0.998	1.010	1.030	0.776
0.6	0.5	0.20	0.10	0.133	0.005	0.129	0.70	0.700	0.701	0.700	0.700	0.701	0.711	0.707	0.787	0.999	1.010	1.028	0.841
0.6	0.5	0.20	0.10	0.150	0.03	0.124	0.50	0.501	0.533	0.511	0.521	0.535	0.552	0.558	0.686	0.973	1.010	1.034	0.736
0.6	0.5	0.20	0.10	0.147	0.03	0.121	0.60	0.601	0.629	0.610	0.618	0.630	0.646	0.649	0.753	0.981	1.010	1.029	0.798
0.6	0.5	0.20	0.10	0.142	0.03	0.115	0.70	0.701	0.724	0.709	0.716	0.726	0.740	0.740	0.820	0.986	1.010	1.026	0.858
0.6	0.3	0.20	0.10	0.113	0.005	0.108	0.50	0.500	0.518	0.500	0.504	0.526	0.554	0.572	0.754	0.959	1.010	1.090	0.770
0.6	0.3	0.20	0.10	0.110	0.005	0.106	0.60	0.600	0.616	0.600	0.604	0.622	0.647	0.660	0.807	0.970	1.010	1.068	0.825
0.6	0.3	0.20	0.10	0.106	0.005	0.101	0.70	0.700	0.714	0.700	0.703	0.719	0.741	0.749	0.860	0.978	1.010	1.051	0.876
0.6	0.3	0.20	0.10	0.100	0.03	0.072	0.50	0.522	0.643	0.565	0.610	0.655	0.686	0.704	0.834	0.931	1.010	1.067	0.853
0.6	0.3	0.20	0.10	0.095	0.03	0.067	0.60	0.622	0.724	0.660	0.697	0.734	0.761	0.773	0.873	0.950	1.010	1.052	0.892
0.6	0.3	0.20	0.10	0.087	0.03	0.059	0.70	0.725	0.808	0.757	0.786	0.815	0.837	0.844	0.914	0.965	1.010	1.038	0.931
0.6	0.5	0	0.08	0.080	0.005	0.076	0.50	0.500	0.545	0.500	0.512	0.551	0.586	0.611	0.794	0.929	1.010	1.107	0.844
0.6	0.5	0	0.08	0.078	0.005	0.073	0.60	0.600	0.639	0.600	0.611	0.644	0.675	0.693	0.839	0.948	1.010	1.080	0.882
0.6	0.5	0	0.08	0.074	0.005	0.069	0.70	0.700	0.734	0.700	0.710	0.737	0.764	0.776	0.884	0.963	1.010	1.058	0.918
0.6	0.5	0	0.08	0.080	0.03	0.052	0.50	0.553	0.693	0.612	0.658	0.703	0.718	0.748	0.859	0.935	0.990	1.038	0.898
0.6	0.5	0	0.08	0.083	0.03	0.055	0.60	0.636	0.745	0.681	0.717	0.753	0.764	0.790	0.882	0.952	0.990	1.026	0.914
0.6	0.5	0	0.08	0.088	0.03	0.060	0.70	0.721	0.799	0.753	0.779	0.806	0.812	0.834	0.906	0.966	0.990	1.015	0.930
0.6	0.3	0	0.08	0.042	0.005	0.037	0.50	0.500	0.710	0.521	0.629	0.726	0.754	0.799	0.914	0.866	0.990	1.066	0.931
0.6	0.3	0	0.08	0.045	0.005	0.040	0.60	0.600	0.758	0.613	0.694	0.771	0.793	0.831	0.927	0.900	0.990	1.049	0.940
0.6	0.3	0	0.08	0.049	0.005	0.044	0.70	0.700	0.807	0.707	0.761	0.818	0.832	0.864	0.940	0.930	0.990	1.034	0.950
0.6	0.3	0	0.08	0.043	0.03	0.014	0.50	0.796	0.901	0.843	0.881	0.907	0.908	0.926	0.959	0.972	0.990	1.006	0.984
0.6	0.3	0	0.08	0.047	0.03	0.017	0.60	0.808	0.905	0.851	0.887	0.911	0.912	0.930	0.962	0.973	0.990	1.006	0.981
0.6	0.3	0	0.08	0.052	0.03	0.023	0.70	0.825	0.911	0.862	0.894	0.917	0.916	0.934	0.965	0.975	0.990	1.005	0.978
0.6	0.5	0	0.12	0.157	0.005	0.153	0.50	0.500	0.501	0.500	0.500	0.503	0.514	0.515	0.645	0.995	1.010	1.045	0.669
0.6	0.5	0	0.12	0.154	0.005	0.149	0.60	0.600	0.601	0.600	0.600	0.603	0.614	0.613	0.720	0.996	1.010	1.038	0.747
0.6	0.5	0	0.12	0.148	0.005	0.144	0.70	0.700	0.701	0.700	0.700	0.702	0.714	0.711	0.795	0.997	1.010	1.033	0.821
0.6	0.5	0	0.12	0.163	0.03	0.137	0.50	0.500	0.524	0.508	0.519	0.538	0.557	0.566	0.694	0.965	1.010	1.047	0.706
0.6	0.5	0	0.12	0.159	0.03	0.133	0.60	0.600	0.621	0.608	0.617	0.633	0.650	0.655	0.759	0.975	1.010	1.038	0.775
0.6	0.5	0	0.12	0.154	0.03	0.128	0.70	0.700	0.719	0.707	0.715	0.727	0.744	0.746	0.825	0.983	1.010	1.032	0.842
0.6	0.3	0	0.12	0.126	0.005	0.121	0.50	0.500	0.515	0.500	0.505	0.531	0.561	0.582	0.757	0.951	1.010	1.098	0.741
0.6	0.3	0	0.12	0.122	0.005	0.118	0.60	0.600	0.614	0.600	0.604	0.627	0.654	0.669	0.810	0.964	1.010	1.073	0.803
0.6	0.3	0	0.12	0.117	0.005	0.113	0.70	0.700	0.712	0.700	0.704	0.723	0.746	0.756	0.862	0.974	1.010	1.054	0.861
0.6	0.3	0	0.12	0.112	0.03	0.085	0.50	0.507	0.619	0.549	0.594	0.644	0.676	0.697	0.826	0.922	1.010	1.074	0.823
0.6	0.3	0	0.12	0.108	0.03	0.080	0.60	0.608	0.704	0.645	0.683	0.724	0.752	0.766	0.867	0.943	1.010	1.057	0.870
0.6	0.3	0	0.12	0.099	0.03	0.072	0.70	0.711	0.791	0.743	0.774	0.805	0.829	0.837	0.909	0.961	1.010	1.042	0.915
0.5	0.5	0	0.10	0.145	0.005	0.141	0.50	0.500	0.501	0.500	0.500	0.505	0.519	0.522	0.666	0.991	1.010	1.060	0.697
0.5	0.5	0	0.10	0.141	0.005	0.136	0.60	0.600	0.601	0.600	0.600	0.604	0.618	0.620	0.738	0.993	1.010	1.049	0.770
0.5	0.5	0	0.10	0.134	0.005	0.130	0.70	0.700	0.701	0.700	0.700	0.704	0.718	0.717	0.810	0.994	1.010	1.040	0.839
0.5	0.5	0	0.10	0.147	0.03	0.120	0.50	0.500	0.534	0.514	0.530	0.554	0.576	0.588	0.722	0.956	1.010	1.061	0.743
0.5	0.5	0	0.10	0.142	0.03	0.116	0.60	0.600	0.631	0.613	0.627	0.648	0.668	0.675	0.783	0.968	1.010	1.048	0.807
0.5	0.5	0	0.10	0.135	0.03	0.109	0.70	0.700	0.728	0.712	0.724	0.741	0.759	0.763	0.845	0.977	1.010	1.038	0.867
0.5	0.3	0	0.10	0.097	0.005	0.093	0.50	0.500	0.539	0.500	0.515	0.563	0.602	0.631	0.806	0.914	1.010	1.113	0.806
0.5	0.3	0	0.10	0.093	0.005	0.089	0.60	0.600	0.635	0.600	0.614	0.656	0.690	0.711	0.850	0.937	1.010	1.084	0.854
0.5	0.3	0	0.10	0.087	0.005	0.083	0.70	0.700	0.733	0.700	0.714	0.748	0.777	0.791	0.894	0.954	1.010	1.061	0.901
0.5	0.3	0	0.10	0.104	0.03	0.077	0.50	0.508	0.635	0.561	0.611	0.665	0.684	0.718	0.841	0.920	0.990	1.051	0.842
0.5	0.3	0	0.10	0.109	0.03	0.081	0.60	0.604	0.699	0.642	0.681	0.723	0.737	0.766	0.867	0.942	0.990	1.035	0.868
0.5	0.3	0	0.10	0.116	0.03	0.089	0.70	0.702	0.763	0.725	0.752	0.782	0.790	0.814	0.893	0.961	0.990	1.021	0.892
0.7	0.5	0	0.10	0.106	0.005	0.102	0.50	0.500	0.517	0.500	0.503	0.521	0.546	0.560	0.738	0.966	1.010	1.083	0.786
0.7	0.5	0	0.10	0.104	0.005	0.099	0.60	0.600	0.615	0.600	0.602	0.618	0.640	0.651	0.793	0.975	1.010	1.063	0.836
0.7	0.5	0	0.10	0.101	0.005	0.096	0.70	0.700	0.713	0.700	0.702	0.715	0.735	0.741	0.849	0.982	1.010	1.048	0.883
0.7	0.5	0	0.10	0.095	0.03	0.067	0.50	0.530	0.647	0.573	0.611	0.654	0.683	0.699	0.825	0.935	1.010	1.064	0.864
0.7	0.5	0	0.10	0.092	0.03	0.064	0.60	0.629	0.725	0.665	0.696	0.731	0.756	0.767	0.865	0.953	1.010	1.050	0.899
0.7	0.5	0	0.10	0.086	0.03	0.058	0.70	0.728	0.805	0.758	0.782	0.809	0.830	0.835	0.906	0.968	1.010	1.037	0.933

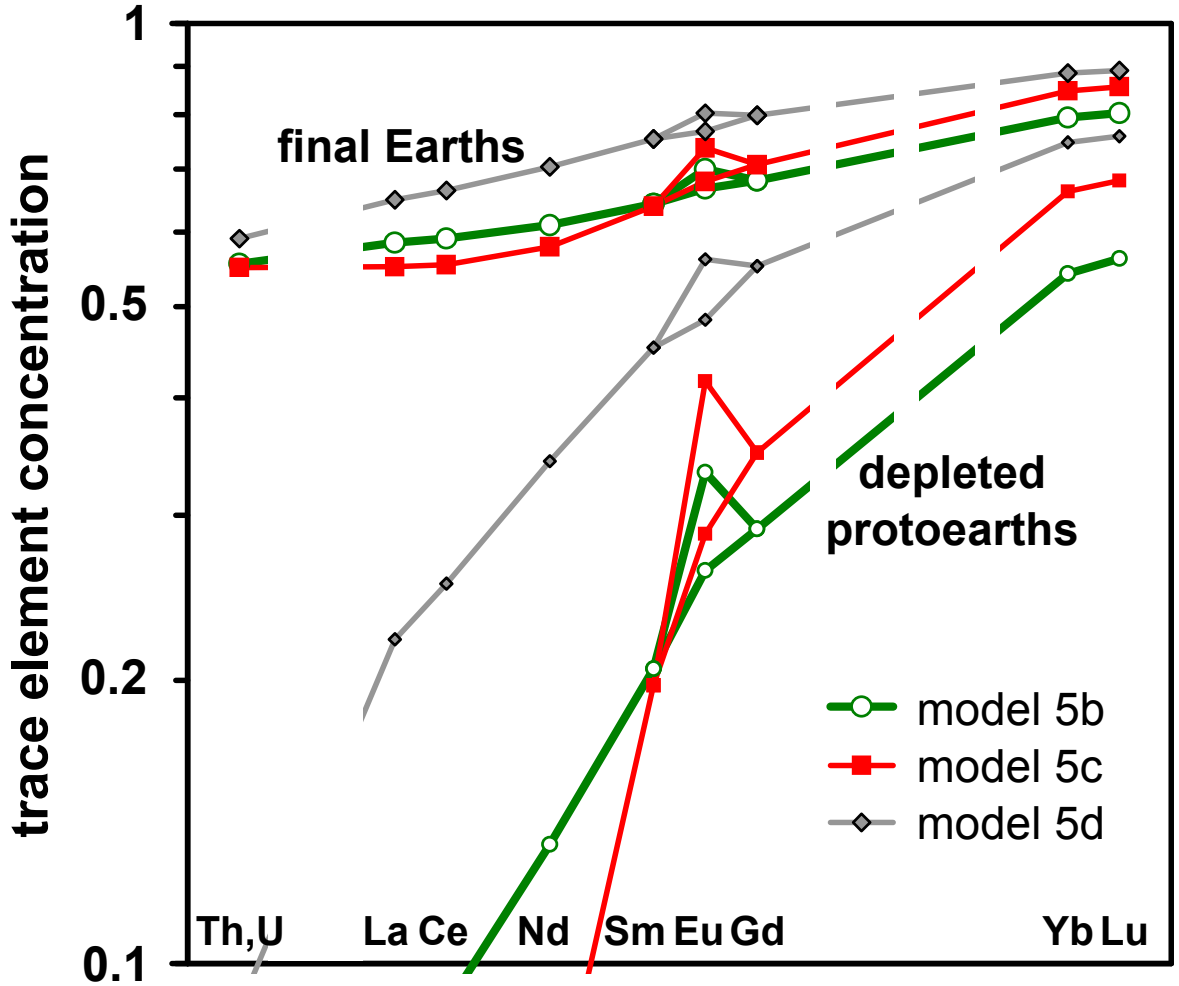

Fig. EA-1. Depletion patterns for REE and Th in three of the same dynamic melting scenarios shown in Fig. 5. Variants shown assume unfractionated component $Y = 0.55$, along with an f that gives Eu/Eu* ≈ 1. Final-Earth Nd/Sm is 0.950, 0.906 and 0.934 in models 5b, 5c and 5d, respectively. Curves are shown for $K_{Eu,plag}$ being both 0.7 and 1.1

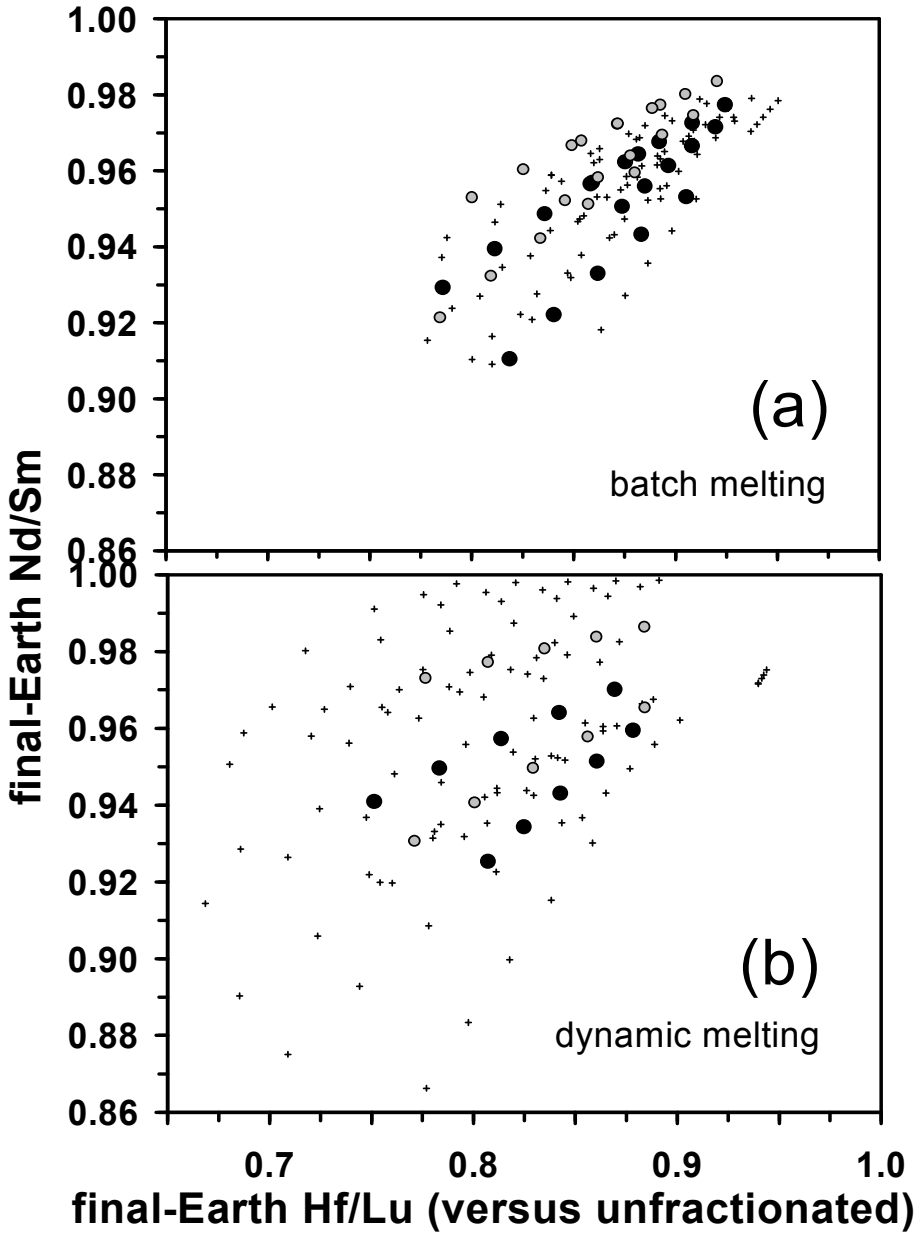

Fig. EA-2. Depletion of Hf/Lu plotted versus final-Earth Nd/Sm for the various models tested (Tables EA-1 and EA-2; also including $Y = 0.55$ and $Y = 0.65$ variants of same models). Largest, darkest symbols denote models close to the "reference" model discussed in the text. Mid-sized symbols represent models that are analogous but assume 20 wt% initial pigeonite, or else a dubiously low porosity ($\Phi = 0.005$) for dynamic melting (b) in a planetesimal context. Smallest symbols denote models that depart most dubiously from the reference model. Caveat: the K set for Hf (adapted from Beard et al., 1998) seems especially uncertain.